Techniques for Diffusion and Perfusion Assessment in Bone-Marrow MRI

Olaf Dietrich

Contents

Abstract

In addition to conventional magnetic resonance imaging (MRI) approaches of bone marrow such as T_1-weighted or short-tau inversion-recovery (STIR) MRI, newer techniques are available today allowing the visual and also quantitative assessment of several microstructural and physiological tissue parameters. The most important of these new techniques are MRI of hemodynamic parameters ("perfusion MRI") and MRI of molecular water diffusion ("diffusion MRI"). Both techniques are aimed at tissue parameters beyond proton density, relaxation properties, or fat content. They allow the (absolute) quantification of properties such as the diffusion coefficient of water molecules in tissue or hemodynamic parameters including the blood volume and the blood flow. In this chapter, the physical and physiological basics of diffusion and perfusion MRI are introduced and discussed with respect to their application in bone-marrow MRI. Non-quantitative and quantitative approaches for the analysis of diffusion-weighted images and semi-quantitative and quantitative approaches for the analysis of dynamic contrast-enhanced perfusion MRI are discussed.

1 Introduction

Magnetic resonance imaging (MRI) is well established for the examination of bone-marrow disorders. Conventional MRI techniques, in particular T_1-weighted MRI with and without contrast-agent administration as well as techniques with fat-signal

O. Dietrich (✉)
Josef Lissner Laboratory for Biomedical Imaging, Department of Clinical Radiology-Großhadern, Ludwig Maximilian University (LMU) of Munich, Munich, Germany
e-mail: od@dtrx.net

A. Baur-Melnyk (ed.), *Magnetic Resonance Imaging of the Bone Marrow*, Medical Radiology. Diagnostic Imaging,
DOI: 10.1007/174_2012_549, © Springer-Verlag Berlin Heidelberg 2013

suppression such as short-tau inversion-recovery (STIR) sequences or fat-saturated proton density-weighted MRI are useful for either the direct visualization of bone marrow or for the sensitive depiction of pathological changes (Glaser et al. 2008). The image contrast of these techniques is based predominantly on the relaxation times (T_1 and T_2) of the magnetization of different types of tissues. Apart from the relaxation properties, the relative fat content of tissue is highly relevant in bone-marrow MRI; therefore, techniques that are sensitive to the fat signal are frequently applied. Examples are techniques which suppress either the fat or the water signal as well as opposed-phase gradient-echo techniques, in which the signal is modulated depending on the relative fat and water content of the tissue (Vanel 2004; Gerdes et al. 2007).

In addition to these conventional approaches, newer techniques are available today allowing the visual and also quantitative assessment of several microstructural and physiological tissue parameters. The most important of these new techniques are MRI of hemodynamic parameters (frequently termed *perfusion MRI*) and MRI of molecular water diffusion (or, shorter, *diffusion MRI*).

Both techniques (diffusion as well as perfusion MRI) are aimed at tissue parameters beyond proton density, relaxation properties, or fat content. They allow the (absolute) quantification of tissue properties such as the diffusion coefficient of water molecules in tissue (in units of mm^2/s) or hemodynamic parameters including the blood (plasma) volume (mL/(100 g)) and the blood (plasma) flow (mL/(min 100 g)). Although both techniques are frequently mentioned and discussed together, it should be noted that they are in fact fundamentally different in their relation to tissue physiology: Diffusion MRI is focused on *physical* parameters (e.g., the diffusion coefficient and its spatial anisotropy), which generally depend in a complicated way on tissue microstructure (such as the cell density and cell types), but can be determined relatively directly from MR measurements. In contrast, perfusion MRI is focused on *physiological* parameters (e.g., plasma volume and flow, tissue transit times), the determination of which is substantially more complicated and generally requires several simplifying assumptions as well as extensive data post-processing. Interestingly, in spite of these principal differences, a suitably performed diffusion MRI measurement can be used to acquire both, diffusion- and perfusion-related tissue parameters together and, thus, reunites both approaches to a certain extent as described below.

In this chapter, the physical and physiological basics of diffusion and perfusion MRI are introduced and discussed with respect to their application in bone-marrow MRI.

2 Principles of Diffusion-Weighted MRI

2.1 Physics of Molecular Diffusion

2.1.1 Diffusion Coefficient

In the context of diffusion MRI, the term *diffusion* refers to the stochastic motion of water molecules in the tissue (Dietrich 2008). It can be directly observed in the form of the Brownian motion of minute particles floating in the liquid. The molecular motion is caused by the thermal kinetic energy and is an undirected random process resulting in a time-varying displacement of each molecule (Fig. 1). Averaged over a large number of molecules, the mean displacement after a certain diffusion time, τ, is 0; i.e., there is no macroscopic (bulk) flow of molecules. However, the standard deviation of the molecular displacements increases with time and, thus, molecular diffusion can be quantified using the statistical variance of displacements $\langle s^2 \rangle$ normalized to the diffusion time to define the diffusion coefficient:

$$D = \frac{\langle s^2 \rangle}{6\tau}.$$

The diffusion coefficient, D, is given in units of mm^2/s, $\mu m^2/ms$, or $\mu m^2/s$. Typical values for biological tissues or liquids are in the order of 1×10^{-3} $mm^2/s = 1$ $\mu m^2/ms = 1{,}000$ $\mu m^2/s$; e.g., pure water has a diffusion coefficient of about 2×10^{-3} mm^2/s at room temperature and of about 3×10^{-3} mm^2/s at body temperature. The diffusion coefficient can be used to estimate the diameter of the spatial range, d, accessible to a water molecule in a given diffusion time, $d \approx 2\sqrt{\langle s^2 \rangle} = 2\sqrt{6D\tau}$. That is, for diffusion times in milliseconds, the diameter given in micrometers can be obtained as $\frac{d}{\mu m} \approx 5\sqrt{\frac{\tau}{ms}}$ based on a diffusion coefficient of 1×10^{-3} mm^2/s. Hence, in vivo, this diameter is in the order of 20–70 μm for typical diffusion times (used in MRI) between 20 and

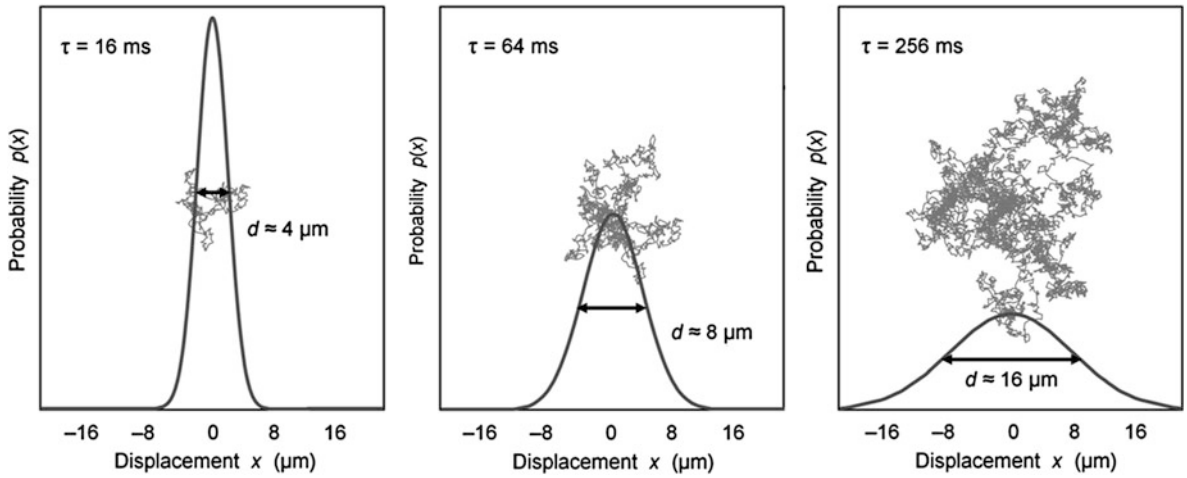

Fig. 1 Molecular diffusion as a microscopic stochastic process. A typical molecular motion of a spin in a liquid (obtained by a random-walk simulation) is illustrated in the background. The probability distribution, $p(x)$, for the resulting displacement is a normal distribution centered at 0. Diffusion times τ increase quadratically from 16 over 64 to 256 ms while the "range", d, of the molecular motion increases linearly from 4 over 8 to 16 µm

200 ms. In other words, an average water molecule in biological tissue will move (stochastically) in a spherical environment with a diameter of about 20 µm during a time interval of 20 ms.

Diffusion coefficients in biological tissue vary between approximately 0 and the value of free water at body temperature depending on the tissue microstructure. This reduction of the measured diffusion coefficient relative to the one of pure water is caused by the interaction of the water molecules with the tissue; e.g., with cell membranes, cell organelles, or biological macromolecules. The motion of the water molecules is hindered to a certain degree by these obstacles and, thus, the molecular displacement is reduced. This effect can increase with the diffusion time, since the number of obstacles hit by a water molecules increases as well. The reduced, effective diffusion coefficient observed in a measurement is called *apparent diffusion coefficient* (ADC). Some typical ADCs are summarized in Table 1.

The value of the ADC depends, thus, on the tissue microstructure; tissues with high cellularity generally exhibit lower ADCs because of the decreased mobility of the water molecules. In contrast, liquids such as the cerebrospinal fluid or necrotic tissues without remaining cell structures exhibit high ADCs similar to the one of pure water.

As mentioned above, the measured ADC of tissue can depend (at least to a certain degree) on the measurement parameters, in particular on the diffusion time, τ, during which the molecules diffuse in the measurement process, but potentially also on other measurement parameters such as the echo time or the application of fat saturation. A closer analysis of the distribution of molecular displacements in tissue for different diffusion times will typically exhibit a more complex form than the originally assumed normal (Gaussian) distribution. Approaches to probe these more complex diffusion properties are, e.g., q-space diffusion analysis (Cohen and Assaf 2002) or diffusional kurtosis

Table 1 Apparent diffusion coefficients (ADCs) of liquids and biological tissues

	ADC (10^{-3} mm^2/s)
Water, 5°C	1.31
Water, 20°C	2.02
Water, 35°C	2.92
Brain, white matter	0.70
Brain, gray matter	0.89
Liver	1.83
Kidney, cortex	2.43
Kidney, medulla	2.16
Vertebral bone marrow	0.2…0.6
Malignant vertebral fracture	0.7…1.0
Osteoporotic vertebral fracture	1.0…2.0

Values from Dietrich (2008), Dietrich et al. (2010) and Dietrich and Baur-Melnyk (2011)

analysis (Jensen and Helpern 2010), which, however, are both beyond the scope of this chapter.

2.1.2 Diffusion Tensor

The stochastic motion of molecules in a liquid is isotropic; i.e., the properties of the motion are independent of the orientation in space. In particular, the standard deviation of the displacement (used for the definition of D) is the same for all directions; e.g., the diffusion coefficient observed along the x direction is the same as the one observed along the y or z or any other oblique direction. However, spatial diffusion anisotropy may be observed in vivo: Anisotropic cell structures, in particular strongly directed tissues such as nerve fibers or muscle fibers, influence the diffusion properties of the water molecules. In such tissues, water diffusion is less restricted parallel to the fiber direction than perpendicular to it and, hence, the measured ADC will be greater along the fiber direction. In this case, the diffusion cannot longer be described by a single diffusion coefficient, but several diffusion coefficients in different spatial orientations are required; this collection of diffusion coefficients is mathematically summarized within the *diffusion tensor*, **D** (Basser et al. 1994a, b). This tensor is described by a symmetric 3×3 matrix and can be obtained in the framework of diffusion tensor imaging (DTI) from a series of diffusion measurements as described below.

While the diffusion tensor itself is a relatively complex entity, certain easily interpretable quantitative parameters can be derived if the tensor is known. These include the mean diffusion coefficient (describing the diffusion averaged over all spatial orientations), different measures of the diffusion anisotropy (e.g., the fractional or relative anisotropy), or the predominant orientation of the diffusion (which typically corresponds to the direction of the cell fibers in the tissue). Many of these parameters are most easily calculated after a process called diagonalization of the diffusion tensor; in this mathematical process, the symmetric 3×3 matrix is transformed to a diagonal matrix with 3 eigenvalues, D_1, D_2, D_3, and to three eigenvectors, $\mathbf{v}_1$, $\mathbf{v}_2$, $\mathbf{v}_3$:

$$\mathbf{D} = \begin{pmatrix} D_{xx} & D_{xy} & D_{xz} \\ D_{xy} & D_{yy} & D_{yz} \\ D_{xz} & D_{yz} & D_{zz} \end{pmatrix} \xrightarrow{\text{diagonalization}} \begin{pmatrix} D_1 & 0 & 0 \\ 0 & D_2 & 0 \\ 0 & 0 & D_3 \end{pmatrix}, \mathbf{v}_1, \mathbf{v}_2, \mathbf{v}_3.$$

The mean diffusivity, D, is then given by the mean value of the three eigenvalues (a third of the *trace* of the diffusion tensor, i.e., of the sum of the eigenvalues or of the diagonal elements):

$$D = \frac{1}{3}(D_1 + D_2 + D_3),$$

the fractional anisotropy (FA), a_F, by (Basser and Pierpaoli 1996)

$$a_{\mathrm{F}} = \sqrt{\frac{3}{2}} \frac{\sqrt{(D_1 - D)^2 + (D_2 - D)^2 + (D_3 - D)^2}}{\sqrt{D_1^2 + D_2^2 + D_3^2}},$$

the relative anisotropy (RA), a_{R}, by

$$a_{\mathrm{R}} = \sqrt{\frac{1}{3}} \frac{\sqrt{(D_1 - D)^2 + (D_2 - D)^2 + (D_3 - D)^2}}{D},$$

and the predominant diffusion direction by the eigenvector belonging to the largest eigenvalue (e.g., by $\mathbf{v}_1$ if $D_1 \geq D_2 \geq D_3$). Both anisotropy measures are dimensionless numbers (i.e., they have no physical units). FA and RA exhibit only minor differences for the description of tissue; they are zero in the case of isotropic diffusion (e.g., in a pure liquid) and increase with growing diffusion anisotropy. The maximum value of the FA (for purely one-dimensional diffusion in a three-dimensional tissue)−− is 1 whereas the maximum value of the RA is $\sqrt{2} \approx 1.414$. (Sometimes, the normalized RA is defined as the RA divided by $\sqrt{2}$; thus also ranging between 0 and 1.)

In particular, for bone marrow or other bone structures, only very few DTI results have been published demonstrating a certain variability of the anisotropy in the spongy bone and a potential of DTI for studying bone architecture (Capuani et al. 2005; Rossi et al. 2005).

2.2 Diffusion-Weighted MRI

2.2.1 Diffusion Weighting of MRI Pulse Sequences

Diffusion MRI is based on the diffusion-related signal attenuation acquired with specifically modified MR pulse sequences: this attenuation increases at higher diffusion coefficients and is caused by a pair of additional gradient pulses (called *diffusion gradients*) in the

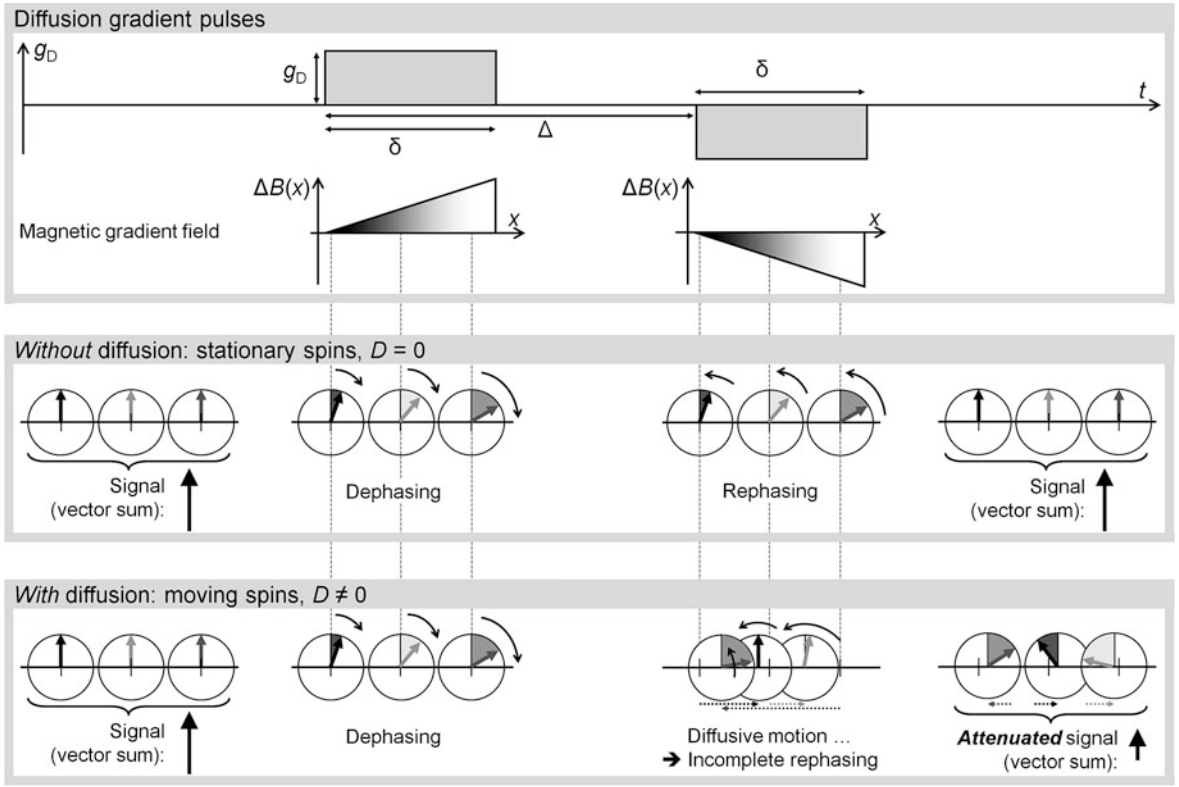

Fig. 2 Signal attenuation by diffusion-weighting gradient pulses. Two gradient pulses, g_D, of duration δ and with an interval of Δ between their onsets cause a spatially varying magnetic field and, thus, influence the phase angle of the precessing spins. Only stationary spins are completely rephased by the second gradient pulse while diffusing spins are rephased incompletely, which is observed as diffusion-attenuated signal intensity

pulse sequence (Hahn 1950; Stejskal and Tanner 1965). The underlying concept is a position-dependent dephasing and rephasing of the nuclear spins: a first gradient pulse modifies the phases of the spins (i.e., the spins are rotated by a certain angle) depending on their position, and a second gradient pulse after the diffusion time, τ, applies exactly the opposite rotation to the spins—if the spins have not moved, but stayed at the same position. If, however, spins have been moving due to the diffusional motion, the applied rephasing cannot fully compensate the initial dephasing and a stochastic phase dispersion remains. This incoherent phase distribution results in a reduced vector sum of individual magnetizations and, hence, in a reduced signal (Fig. 2).

The strength of this attenuation effect is called *diffusion weighting* or *b-value* of the sequence and depends (in the case of two identical gradient pulses) on the gradient amplitude, g_D, the gradient duration, δ, and the interval between the onsets of the gradients, Δ. The diffusion weighting for the pulses shown in Fig. 2 is

$$b = \gamma^2 g_D^2 \delta^2 \left(\Delta - \frac{\delta}{3}\right),$$

where $\gamma = (2\pi) \times 42.58 \times 10^6\ \mathrm{s}^{-1}/\mathrm{T}$ is the gyromagnetic ratio of the precessing nuclei (the given number is the gyromagnetic ratio for protons). The diffusion time, τ, is approximately equal to the interval, Δ, between the onsets of the diffusion gradients; in the case of relatively long diffusion gradients, the gradient duration, δ, needs to be considered as well, yielding a corrected diffusion time of $\tau = \Delta - \frac{\delta}{3}$. More generally, for arbitrary gradient shapes $g(t)$ in a given orientation applied between times $t = 0$ and $t = T$, the b-value is given by the integral:

$$b = \gamma^2 \int_{t=0}^{T} \left(\int_{t'=0}^{t} g(t')\mathrm{d}t' \right)^2 \mathrm{d}t.$$

Typical (maximum) b-values for conventional clinical diffusion MRI are in the range of 500–1500 s/mm^2.

The signal attenuation of a diffusion-weighted acquisition depends exponentially on the b-value and the diffusion coefficient, D (similarly as the signal attenuation in a T_2-weighted acquisition depends on the echo time, TE, and on the relaxation rate $R_2 = 1/T_2$). The attenuation $S(b)/S_0$ (relative to the original signal amplitude S_0) is

$$\frac{S(b)}{S_0} = \exp(-b \cdot D).$$

Higher attenuations correspond to larger diffusion coefficients and vice versa; thus, diffusion-weighted images show regions with reduced ADCs (such as ischemic brain tissue in stroke patients or tumor tissue with increased cellularity) hyperintense compared to normal-appearing tissue.

The diffusion coefficient can be determined quantitatively by measuring the attenuation, $S(b)/S_0$, for two or more different b-values and then fitting the exponential function to the measured signals. In the simplest case of only two measurements with b-values 0 and b, the ADC can also be calculated directly from the logarithm of the signal attenuation as

$$D = \frac{-1}{b} \ln \frac{S(b)}{S_0}.$$

Areas with reduced ADC that appear hyperintense in diffusion-weighted images are hypointense in the ADC map.

With the technique described above, the diffusion coefficient can be measured in the orientation of the applied diffusion gradient. The components of the diffusion tensor are measured by applying the diffusion gradient in several different spatial orientations (measurements in at least 6 non coplanar diffusion directions are required to estimate all 6 independent components of the tensor (Basser and Pierpaoli 1998)).

2.2.2 Pulse Sequences for Diffusion-Weighted MRI

Diffusion gradients as described above can be inserted in many different MRI pulse sequence types as summarized, e.g., in Dietrich et al. (2010) or Dietrich and Baur–Melnyk (2011). Historically, the first diffusion-weighted MR images were acquired with (single-echo) stimulated-echo and spin-echo sequences (Merboldt et al. 1985; Taylor and Bushell 1985; Le Bihan et al. 1986), which, however, were very slow and prone to motion artifacts. Today, the most important sequence type for diffusion-weighted imaging (DWI) is the single-shot spin-echo echo-planar imaging (EPI) sequence, in which the diffusion gradients can be easily inserted at both sides of the 180° refocusing radio-frequency (RF) pulse (Turner et al. 1990). EPI acquisitions are fast (a complete image can be acquired in about 0.2 s) and, hence, relatively insensitive to motion. On the other hand, EPI sequences are very sensitive to susceptibility variations and eddy currents, both potentially resulting in geometrically gross distortions of the images. Diffusion-weighted EPI sequences have been established for many years for imaging of the brain (where only moderate susceptibility artifacts occur); but only relatively recent improvements of MRI hardware and in particular of the gradient system and the fat-suppression techniques enabled the general robust application of diffusion-weighted MRI in many other parts of the body and, in fact, also for whole-body applications (Takahara et al. 2004; Lambregts et al. 2011; Wu et al. 2011).

Other fast techniques for diffusion MRI are single-shot fast-spin-echo (or turbo-spin-echo) sequences with additional diffusion gradients such as diffusion-weighted half-Fourier-acquisition single-shot turbo-spin-echo (HASTE) or rapid acquisition with relaxation enhancement (RARE) sequences (Norris et al. 1992). These approaches avoid the high sensitivity to susceptibility variations of EPI sequences, but they exhibit certain other disadvantages including lower signal-to-noise ratio (SNR) or image artifacts due to unwanted stimulated echoes. Several detail improvements have been proposed to increase the image quality and robustness of these pulse sequences for diffusion-weighted MRI (Alsop 1997; Le Roux 2002; Norris 2007).

Further and less frequently applied approaches include segmented (multi-shot) EPI techniques (Robson et al. 1997; Brockstedt et al. 2000), non-Cartesian k-space trajectories with radial acquisition or with the "periodically rotated overlapping parallel lines with enhanced reconstruction" (PROPELLER) technique (Pipe et al. 2002), diffusion-sensitized fast spoiled gradient-echo (turbo-FLASH or snapshot-FLASH) sequences (Lee and Price 1994) or line-scan diffusion-weighted imaging sequences (Gudbjartsson et al. 1996).

A somewhat different approach for diffusion-weighted imaging is obtained by inserting a single diffusion gradient in a steady-state free-precession

(SSFP) sequence. SSFP sequences can be differentiated in three different basic types: those that acquire a free-induction-decay(-FID)-like signal such as the "Fourier-acquired steady-state" (FAST) or "fast imaging with steady precession" (FISP) sequences; those with a spin-echo-like signal such as the contrast-enhanced FAST (CE-FAST) or the reversed FISP (PSIF) sequences; and finally those with fully balanced gradients that acquire a combination of both signals such as the TrueFISP or balanced SSFP (bSSFP) sequences (Oppelt et al. 1986; Bruder et al. 1988; Gyngell 1988). To obtain a reasonable diffusion weighting at short repetition times (TR), particularly the spin-echo-like approaches have proven useful (Le Bihan 1988; Merboldt et al. 1989). Inserting a single (monopolar) diffusion gradient in each TR provides a spin dephasing that is rephased at a later TR (not necessarily at the immediately successive one since the magnetization is switched around between transversal and longitudinal contributions). The delayed rephasing is advantageous in that it provides an increased diffusion weighting—however, it becomes extremely complicated to exactly quantify the diffusion weighting, since it depends not only on the properties of the diffusion gradient, but also on the flip angle, the TR, and the relaxation times of the tissue (Wu and Buxton 1990; Buxton 1993; Deoni et al. 2004). Therefore, diffusion-sensitized SSFP sequences can be used to acquire diffusion-weighted image data (which qualitatively visualize increased ADCs as attenuated signal), but not for the exact quantification of diffusion coefficients. This approach has been demonstrated to be particularly valuable in vertebral bone marrow, since a differentiation of pathological (neoplastic) and benign (osteoporotic) vertebral compression fractures is possible based on the contrast of the diffusion-weighted PSIF sequence (Baur et al. 1998, 2001; Dietrich et al. 2009; Biffar et al. 2011a, b; Dietrich and Baur-Melnyk 2011).

2.3 Diffusion-Weighted MRI in Bone Marrow

When diffusion-sensitive MR techniques are to be applied in bone marrow, the choice of the pulse sequence type and of several sequence parameters should, in general, be different from those used, e.g., for diffusion-weighted MRI of the brain. While echo-planar imaging is the standard technique for diffusion measurements in the brain, a broader spectrum of techniques is applied in body applications. Typically, the homogeneity of the static magnetic field (B_0) is lower in body applications than in the brain, resulting in severer geometrical distortions and image artifacts due to impaired fat suppression when using echo-planar imaging. Thus, pulse sequences with reduced sensitivity to field inhomogeneities have often been applied for bone-marrow imaging such as diffusion-weighted RARE or line-scan diffusion-weighted imaging sequences (Dietrich et al. 2009; Dietrich and Baur-Melnyk 2011).

The transversal relaxation times (T_2) are typically shorter in the musculoskeletal system than in the brain and, hence, the signal intensity is frequently low due to the relatively long echo times required for diffusion-weighted sequences. To obtain sufficient signal, multiple averaging and shorter echo times should be used implying also a reduced maximum diffusion weighting of, e.g., only $b = 600$ s/mm^2 instead of 1,000 s/mm^2.

On the other hand, typical ADCs of normal bone marrow are substantially lower (by a factor of 2–3) than of the brain or of abdominal organs; published values range between about 0.2 and 0.6 $\times$ 10^{-3} mm^2/s. Due to these low ADCs and the technical constraints mentioned above, it is very difficult to measure the ADCs of bone marrow accurately in a reasonable scan time. This is also reflected by the considerable variation of published ADCs of bone marrow as summarized in (Dietrich et al. 2009; Dietrich and Baur-Melnyk 2011). Apart from image noise, these varying results are also influenced by the choice of applied b-values as well as by the application fat saturation. Fortunately, ADCs of most bone-marrow pathologies are generally significantly higher (cf. Table 1) and, thus, can be detected much more accurately even at low b-values.

3 Principles of Perfusion MRI

3.1 Hemodynamic Tissue Properties

In the context of perfusion MRI, the term *perfusion* is frequently used (pars pro toto) to summarize several hemodynamic parameters associated with the (capillary) blood supply of biological tissue. These include the blood volume in the tissue, the blood flow and typical transit time constants. Depending on the physiology, these parameters can be defined and measured

for a single physiological compartment or for multiple tissue compartments with certain exchange properties (Brix et al. 2010; Sourbron 2010; Sourbron and Buckley 2012). In a narrower definition, perfusion is used as synonym for the blood flow parameter and is, thus, one of several hemodynamic parameters.

The hemodynamic parameters mentioned above were traditionally defined (and measured) on a per-organ basis by considering the total blood flow through an organ (in units of mL/min) or the corresponding total blood volume (in mL). For instance, typical organ perfusion values (in rest) are about 250 mL/min for the myocardium, 750 mL/min for the brain, and 1200 mL/min for the kidneys. Dividing these values by the mass (or the volume) of the organ, the average specific tissue perfusion is calculated. Typical values are 4 mL/(min g) = 400 mL/(min 100 g) for the kidney parenchyma or 0.5 mL/(min g) =50 mL/(min 100 g) for brain tissue (Silbernagl and Despopoulos 2008).

With imaging methods, hemodynamic parameters can be determined spatially resolved for the tissue of an organ. These values are defined as before normalized to the mass or volume of perfused tissue, but may now exhibit regional differences, e.g., for gray and white matter of the brain or for the renal cortex and the medulla. In this case, the regional flow is also given in units of mL/(min 100 g) or mL/(min 100 mL) and the regional blood volume in units of mL/(100 g) or mL/(100 mL). The conversion factor between both conventions (normalization to mass or volume) is the specific tissue mass density, ρ, in units of g/cm^3 = g/mL, which is relatively close to 1 g/mL for several soft tissues (with certain exceptions such as the lung). Thus, a regional kidney perfusion of about 400 mL/(min 100 g) based on the mass of the tissue is approximately equivalent to a flow value of 400 mL/(min 100 mL) if normalized to the volume.[1]

3.2 Techniques for Perfusion MRI

Perfusion MRI can be performed qualitatively or quantitatively with several fundamentally different techniques. The most important approaches are either based on the administration of intravenous contrast-media or—employing blood as an endogenous contrast-agent—on the labeling of arterial blood by appropriate magnetization preparation RF pulses, the so-called arterial spin labeling (ASL) techniques (Luypaert et al. 2001; Petersen et al. 2006). A third approach is based on diffusion-weighted acquisitions: The signal attenuation of diffusion-weighted images at very low *b*-values between 0 and about 150 s/mm^2 is influenced by the microcapillary perfusion as well as by normal diffusive processes. This additional influence results in a bi-exponential signal attenuation instead of the mono-exponential dependence described above. By analyzing the bi-exponential signal, two characteristic parameters, the perfusion fraction (in percent) and the perfusion-related pseudo diffusion coefficient, D^*, can be determined. This technique is frequently called *intravoxel incoherent motion* (IVIM) MRI and was already proposed in the 1980s (Le Bihan et al. 1988), but only recently, the general interest in this kind of acquisition has grown substantially (Koh et al. 2011).

Perfusion techniques that are based on the administration of an exogenous contrast-agent can be grouped into those that acquire the signal attenuation in T_2^*-weighted acquisitions due to the contrast-agent susceptibility ("dynamic susceptibility-contrast-enhanced MRI", DSC-MRI) (Ostergaard 2004) and those that acquire the contrast-media-induced signal increase in T_1-weighted acquisitions (Jackson et al. 2005). For bone-marrow MRI, only the last approach has been applied in a relevant number of studies; hence, the remaining parts of this introduction focus on these contrast-enhanced T_1-based techniques.

Depending on the specific acquisition parameters of the T_1-weighted measurement, particularly on the number of acquisitions and their temporal resolution, the evaluation of tissue perfusion can be performed either only qualitatively, semiquantitatively, or fully quantitatively yielding absolute hemodynamic parameters. The acquisition requirements are lowest if only a qualitative evaluation is intended. Even a single T_1-weighted acquisition after contrast-media injection will reflect certain perfusion-related properties: contrast enhancement is generally associated with blood volume and flow, and regions without perfusion are not enhanced at all. However, even a qualitative evaluation of perfusion properties is usually based on the signal development in several

[1] If normalized to the volume, the regional blood volume can also be given in % = mL/(100 mL) and the regional flow-related quantities in %/min = mL/(100 mL min).

subsequent acquisitions with temporal resolutions ranging from seconds to some minutes. Techniques that acquire such T_1-weighted signal-time courses are referred to as dynamic contrast-enhanced MRI (DCE-MRI) (Dyke and Aaron 2010; Sourbron 2010).

Only at high temporal resolutions of ideally about 1–3 s per acquisition, the details of the contrast-media passage through the vasculature can be analyzed, which is required for an accurate evaluation of the associated blood-flow parameters. Acquisitions with lower temporal resolutions, i.e., with reduced data acquisition rate, can be used to evaluate only a subset of hemodynamic parameters such as the contrast-media extravasation into the tissue if the total acquisition duration is sufficiently long.

By far the most commonly used sequence type for T_1-weighted perfusion MRI is the fast spoiled gradient-echo technique or, synonymously, fast low-angle shot (FLASH) or fast field-echo (FFE) sequence (Sourbron 2010). This sequence type can be used either for two-dimensional or three-dimensional acquisitions and with or without magnetization preparation such as inversion or saturation pulses. Frequently found combinations are saturation-recovery turbo-FLASH (snapshot-FLASH) sequences with short saturation times of 100–200 ms and two-dimensional readout, or three-dimensional gradient-echo sequences without magnetization preparation. Of particular importance for (semi)quantitative evaluations is a high temporal resolution of the acquisition in the order of about 1–3 s per acquisition. In two-dimensional approaches, this is achieved by relatively low spatial resolutions, high receiver bandwidth and very short TRs, a low number of acquired slices, and several acceleration techniques such as partial-Fourier acquisitions or parallel imaging. Fast, dynamic three-dimensional imaging is optimized similarly with relatively low spatial resolutions and parallel-imaging approaches; in addition, with view-sharing techniques (e.g., "time-resolved imaging of contrast kinetics", TRICKS, or "time-resolved imaging with stochastic trajectories", TWIST) that update the center of k-space more frequently than the periphery can be employed (Korosec et al. 1996; Lim et al. 2008). The sequence parameters, in particular the saturation time and the flip angle, should be chosen such that the resulting signal enhancement is approximately proportional to the contrast-agent concentration for those concentrations typically found in arteries and perfused tissue.

Apart from the pulse sequence, the contrast-media injection protocol needs to be considered and optimized for perfusion MRI. Typically, a standard dose of contrast-agent (0.1 mmol/kg body weight) is injected as a short bolus followed by a saline flush of about 20–30 mL. Injection rates are about 3 mL/s resulting in an injection duration of approximately 5 s for a typical contrast-agent.

3.3 Evaluation of Perfusion MRI

3.3.1 Qualitative and Semiquantitative DCE-MRI

A simple qualitative evaluation of the tissue perfusion can be based on the visual inspection of the signal-time course in a dynamic series of T_1-weighted images. A regionally increased signal enhancement indicates hyperperfused tissue, while a decreased enhancement is associated with hypoperfused tissue; a typical example of the latter is the locally reduced visual enhancement of lung parenchyma after thromboembolic arterial occlusion. If a series of several dynamic phases (e.g. 6–10) is acquired with a temporal resolution between 15 s and 1 min, it might be possible to differentiate qualitatively several enhancement patterns (in particular slowly increasing enhancement associated with the extravasation of the contrast-agent vs. fast contrast-agent wash-out in later phases). For instance, two enhancement types, namely one with a considerable wash-out after the initial rise of contrast and the other one with a plateau at the later phase, were differentiated in a study of degenerative endplate marrow changes based on a series of nine acquisitions with a temporal resolution of 16.4 s (Savvopoulou et al. 2011). The analysis of enhancement patterns or time-intensity curve (TIC) patterns can also be applied at higher temporal resolutions: e.g., in a perfusion study of vertebral lesions, five evaluated TIC patterns were "nearly no enhancement", "slow enhancement", "rapid contrast wash-in followed by an equilibrium phase", "rapid contrast wash-in followed by early wash-out", and "rapid contrast wash-in with a second slower-rising slope" (Chen et al. 2002).

Qualitative evaluations can be performed visually without the need for any dedicated software; however, the results are generally difficult to compare inter- or intra-individually (e.g., between baseline and follow-up examinations). The requirements with respect to

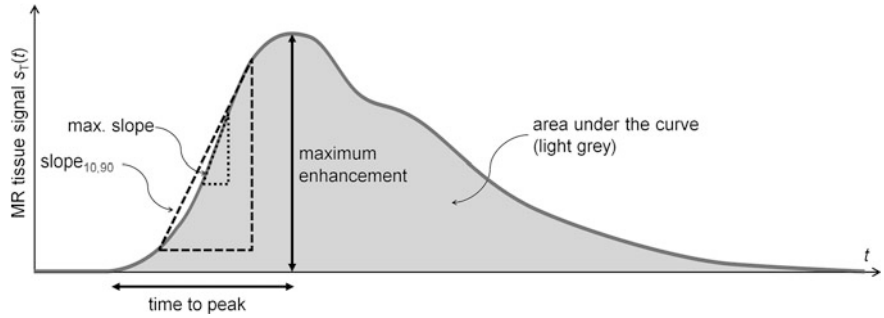

Fig. 3 Descriptive (semi-quantitative) perfusion parameters. Shown is the (idealized) signal-time curve of the tissue of interest obtained, e.g., by evaluating the mean signal of a region of interest. Important descriptive parameters of this curve are the maximum (or peak) enhancement, the time to peak, the area under the curve, or the slope which can be determined either by evaluating the difference between 10 and 90% of the maximum signal enhancement ($slope_{10,90}$) or by estimating the maximum slope

the applied imaging technique (in particular, to the temporal resolution and to signal linearity) are relatively low.

More information than by visual inspection can be obtained from DCE-MRI measurements with sufficient temporal resolution by deriving several descriptive or semiquantitative parameters from the acquired signal-time curves (Fig. 3). The most important of these parameters are the maximum of the curve (peak enhancement), the time to peak, the area under the curve, or the (maximum) slope of the signal increase. There are several options for the calculation of the slope; e.g., it can be estimated from the enhancement rate between 10 and 90% of the total enhancement (from baseline to maximum signal). Semiquantitative parameters were evaluated in several recent publications on bone-marrow perfusion (Griffith et al. 2009; Chan et al. 2011; Courcoutsakis et al. 2011; Li et al 2012).

The two main disadvantages of these descriptive parameters are their obvious dependence on the experimental parameters such as the pulse sequence contrast and, in particular, on the contrast-agent injection protocol as well as their unclear interpretation in terms of physiological hemodynamic terms. Depending on the tissue and the pathology (e.g. tumor or ischemia), the relationship between the descriptive parameters and the physiological parameters such as the blood flow into the tissue or the diffusion of fluid into the extracellular space can be very different. In studies based on these semiquantitative (descriptive) parameters, it is frequently left open exactly which hemodynamic tissue property is examined.

On the other hand, obvious advantages of many of these descriptive parameters are that they are reasonably easy to calculate and relatively robust even in the presence of noise.

3.3.2 Quantitative DCE-MRI

Apart from the descriptive indices mentioned above, it is also possible to estimate several quantitative hemodynamic parameters such as the regional blood volume (RBV), the regional blood flow (RBF), or the permeability-surface-area product (PS) describing the vascular permeability (i.e., the extraction flow) from a detailed analysis of the measured contrast-agent dynamics. To obtain parameters that do not depend on the (variable) injection and circulation parameters and, thus, on the individual shape of the contrast bolus, this analysis has to be based on the contrast-agent dynamics in two regions: (1) in the tissue of interest and (2) in the tissue-feeding artery. The background of this procedure in the framework of indicator-dilution theory (Meier and Zierler 1954; Zierler 1962, 1965; Sourbron and Buckley 2012) is explained in Fig. 4: The contrast-agent concentration-time curve in the tissue, $c_T(t)$, is a complex combination of a tissue-response function (or impulse-response function), $f_T(t)$, and the arterial input function (AIF), $c_A(t)$. In the case of an idealized extremely short contrast-agent input as in Fig. 4a, the tissue-response, i.e., the concentration-time curve in the tissue, is directly given by the tissue-response function. The tissue-response function contains all hemodynamic information related to the tissue: Its initial value, $f_T(0)$, is the blood flow through the tissue and the area

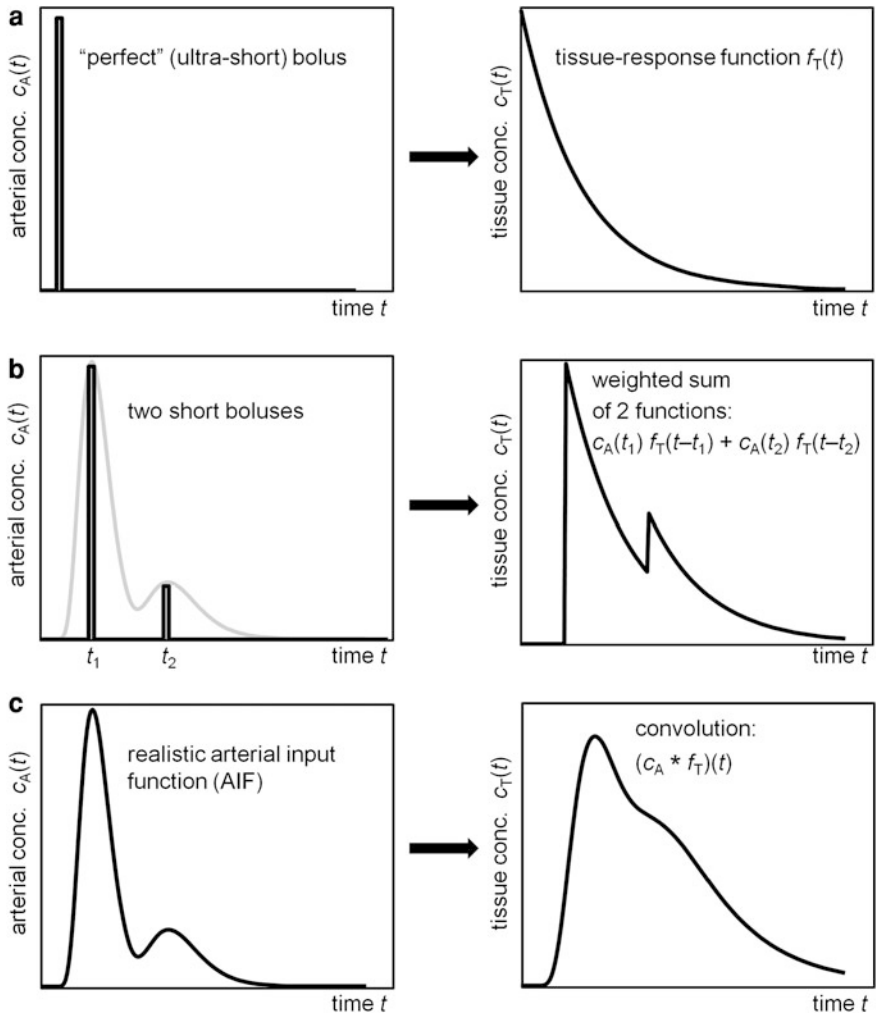

Fig. 4 Tissue concentration-time curve as a convolution of arterial concentration and tissue-response function. **a** The tissue-response function describes the contrast-agent concentration in the tissue after a "perfect" (extremely short) arterial bolus. **b** If the arterial input function (AIF, gray) is approximated by two boluses for the first pass and the re-circulation, the tissue concentration is obtained by the sum of two shifted tissue-response functions. **c** In the case of a realistic AIF, the sum is replaced by an integral, i.e., by the convolution of AIF and tissue-response function

under the curve, $\int_{-\infty}^{\infty} f_T(t)\mathrm{d}t$, is the blood volume in the tissue. A third important parameter, the mean transit time (MTT) is given by the quotient $\int_{-\infty}^{\infty} f_T(t)\mathrm{d}t / f_T(0)$. Depending on the tissue physiology, further parameters such as the permeability-surface-area product (extraction flow) or the extravascular, extracellular volume may also be required to describe the tissue-response function, and, thus, may be derived from this function. Hence, the tissue-response function may be written as $f_T(t; A,B,C,\ldots)$, where A, B, C, … describe several hemodynamic tissue parameters that influence the tissue response.

If the tissue-response function is normalized to the initial value 1, i.e., divided by the blood flow, $f_T(0)$, the resulting function, $R(t) = f_T(t) / f_T(0)$, is called the tissue-residue function. This function (and thus, practically, the tissue-response function itself as well) has the following simple interpretation: the residue functions describes what fraction of the blood (or contrast-agent) pool present in the tissue at $t = 0$ is still there at the time t. I.e., if we label the blood in the tissue at an arbitrary point of time and then wait the interval, t, exactly the fraction $R(t)$ (< 1) of the originally labeled blood is still there. Consequently, the residue function is always a positive and monotonically decreasing function.

An important approach to measure the above-mentioned hemodynamic parameters is the determination of the tissue-response function in an organ. However, if the bolus is not an ideal, ultra-short

impulse but a realistic bolus, then the influence of the bolus shape has to be removed from the concentration-time curve in the tissue. To understand this influence, one can imagine a sequence of short pulses with amplitude $c_A(t_i)$ at time t_i as approximation to the realistic arterial bolus shape as shown in Fig. 4b. The resulting concentration-time curve is then a superposition of several shifted tissue-response functions scaled by the amplitude of the individual impulses:

$$c_T(t) = c_A(t_1) \cdot f_T(t - t_1) + c_A(t_2) \cdot f_T(t - t_2) + \cdots = \sum_{i=1}^{N} c_A(t_i) \cdot f_T(t - t_i)$$

The transition to a smooth arterial input function (see Fig. 4c) is now equivalent to an integral calculation (instead of the sum of functions), called the *convolution* of the arterial input function and the tissue-response function (denoted by the symbol *):

$$c_T(t) = \int_{-\infty}^{\infty} c_A(s) \cdot f_T(t - s)ds = (c_A * f_T)(t).$$

In a typical perfusion measurement, the tissue concentration $c_T(t)$ and the arterial input concentration $c_A(t)$ are measured and the tissue-response function, $f_T(t)$ (or the parameters $A, B, C, \ldots$ defining $f_T(t)$), are to be determined from these; i.e., the convolution process has to be inverted. This calculation is termed deconvolution and sometimes denoted by the symbol $*^{-1}$:

$$f_T(t) = \left(c_T *^{-1} c_A\right)(t).$$

Unfortunately, the direct deconvolution is a numerically difficult and not very robust process (also called a numerically ill-posed problem) and several so-called regularization strategies have been proposed to improve the deconvolution such as truncated singular-value decomposition or the standard-form Tikhonov regularization (Kind et al. 2010).

An alternative to the direct deconvolution approach is based on a tissue model with a number of hemodynamic parameters A, B, C, … that imply a certain mathematical form of the tissue-response function, $f_T(t; A,B,C,\ldots)$. By varying these parameters, the convolution $(c_A * f_T)(t; A, B, C, \ldots)$ can be calculated and compared with the actual concentration, $c_T(t)$, in the tissue. By minimizing the difference

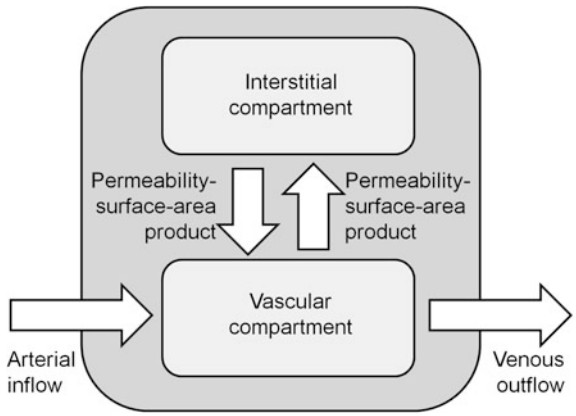

Fig. 5 Two-compartment exchange model with vascular and interstitial compartment. Four parameters that can be used to describe this model quantitatively are the (arterial) blood flow into the vascular compartment, the blood volumes of each compartment, and the flow (extraction flow or, synonymously, permeability-surface-area product) between the two compartments

(defined as the sum of squared differences) between the calculated convolution and the measured concentration-time curve, the hemodynamic parameters A, B, C, … are determined. This least-squares fitting procedure is frequently performed with the Levenberg–Marquardt algorithm.

The tissue model can comprise one or more (frequently two) compartments with certain individual properties such as specific blood volumes or specific mean transit times. A tissue compartment is generally defined as a space in which the contrast-agent is distributed instantly and uniformly and which has an inlet and an outlet connected to other compartments. A typical two-compartment model includes, e.g., the vascular compartment with arterial inflow and venous outflow as well as an extravascular, extracellular (i.e., interstitial) compartment to which blood (and contrast-agent) is transported via the permeable vascular surface, described by the permeability-surface-area product. A frequently used quite general model is the two-compartment exchange model with bidirectional flow between both compartments (Fig. 5).

Under certain conditions, the blood volume and flow can also be estimated directly from the tissue concentration and the AIF without the need for numerical deconvolution. E.g., the blood volume is given by $\int_0^\infty c_T(t)\mathrm{d}t / \int_0^\infty c_A(t)\mathrm{d}t$, if the concentration-time curves return to zero within the acquisition window.

All considerations above were based on the *concentration*-time curves (in the artery or the tissue); these, however, are not directly accessible in MRI but must be derived from the measured *signal*-time curves. Depending on the pulse sequence type and other parameters such as the flip angle distribution, different relationships between either the absolute or relative signal enhancement due to the contrast-media and the contrast-media concentration can be established. In most situations, additional calibration measurements of the pre-contrast T_1 values and the B_1 (flip angle) homogeneity are required (Sourbron 2010).

3.4 Perfusion Parameters in Bone Marrow

Perfusion properties of bone marrow have been assessed at least qualitatively or semiquantitatively in a relatively large number of studies as summarized, e.g., in (Biffar et al. 2010a). Early examinations of contrast-media uptake dynamics in bone tumors were already performed in the late 1980s demonstrating higher slopes of enhancement in malignant than in benign bone tumors (Erlemann et al. 1989). Further semiquantitative analyses demonstrated, e.g., decreasing bone-marrow perfusion with age (Chen et al. 2001; Montazel et al. 2003) or with osteoporosis (Shih et al. 2004; Griffith et al. 2005). Increasing perfusion indices were demonstrated, e.g., in bone marrow with diffuse tumor infiltration (Rahmouni et al. 2003), in myeloproliferative neoplasms (Courcoutsakis et al. 2011), in idiopathic osteonecrosis of the femoral head (Chan et al. 2011), and in rheumatoid arthritis (Li et al. 2011); increasing contrast enhancement and lower slopes were reported for degenerative endplate changes (Savvopoulou et al. 2011). Reduced perfusion indices at baseline were shown to predict increased reduction of the bone mineral density in the femoral neck after 4 years (Griffith et al. 2011). Significantly different semiquantitative perfusion parameters were found in neoplastic and normal bone (D'Agostino et al. 2010) as well as in osteoporotic and neoplastic vertebral compression fractures (Tokuda et al. 2005); for the latter differentiation, time-intensity-curve patterns were also reported to be valuable (Chen et al. 2002). Another recent study showed a generally good reproducibility of the measurement of these perfusion-related indices in the bone (Griffith et al. 2009).

Only few results have been published with fully quantitative perfusion evaluation of the bone marrow. Permeability-related quantitative parameters of bone marrow evaluated in patients with multiple myeloma yielded increased values for the contrast-agent exchange rate constant of tissue with (high-degree) infiltration (Moehler et al. 2001; Nosas-Garcia et al. 2005). Permeability constants, elimination rates, and the perfusion amplitude were found to be reduced in osteoporotic subjects using a modified Brix model (Ma et al. 2010) and increased in bone marrow edema relative to normal bone (Lee et al. 2009). Typical blood flow and volume parameters in normal-appearing vertebral bone marrow are reported to be about 15 mL/(100 mL min) and about 5 mL/100 mL, respectively, with a very low permeability-surface-area product (Biffar et al. 2010b, 2011b). These values are significantly increased in osteoporotic vertebral fractures as summarized in Table 2. An improved analysis of bone-marrow perfusion data has been proposed to include effects of the fat fraction within the tissue which is about 30–50 % in healthy bone marrow (Biffar et al. 2010c). Assuming that the contrast-agent influences only the T_1 relaxation of the water protons and considering the different baseline relaxation rates of the fat and water fraction in bone marrow, this more sophisticated perfusion analysis yielded a significantly increased value of plasma volume in healthy bone marrow and a significantly decreased value of plasma flow in vertebral fractures (Table 2).

4 Conclusions

Both diffusion and perfusion MRI have been successfully employed for bone-marrow imaging studies in a multitude of different pathologies. A large number of these studies apply conventional diffusion-weighted imaging in order to determine apparent diffusion coefficients in bone marrow or, alternatively, to assess pathologies based on relative signal attenuations, e.g., using diffusion-weighted SSFP techniques. Frequently employed approaches for perfusion MRI are based on descriptive perfusion indices such as peak enhancement or slope derived directly from the signal-time

Table 2 Quantitative perfusion parameters in vertebral bone marrow

	Plasma flow (mL/(min 100 mL))	Plasma volume (mL/100 mL)	Permeability-surface-area product (mL/(min 100 mL))	Interstitial volume (mL/100 mL)	Ref.
Normal-appearing bone marrow	15	5	–	–	[a]
	18	6	0.1	–	[b]
	17	10	0.3	–	[c]
Osteoporotic fractures	71	25	20	28	[a]
	69	24	10	20	[b]
Osteoporotic or malignant fractures	41	21	6	19	[c]
	67	20	7	19	[d]

[a] Biffar et al. (2010b)
[b] Biffar et al. (2011b)
[c] Perfusion quantification considering the fat fraction in bone marrow (Biffar et al. 2010c)
[d] Perfusion quantification without considering the fat fraction (Biffar et al. 2010c)

curves of dynamic contrast-enhanced T_1-weighted acquisitions in different tissues of interest.

Newer diffusion techniques including diffusion tensor imaging, intravoxel incoherent motion MRI, or generalized non-Gaussian diffusion methods may be promising, but are not yet systematically evaluated in bone-marrow applications. Similarly, a fully quantitative perfusion assessment with appropriate multi-compartment models has been evaluated only in a very small number of recent studies. These techniques still promise improved diagnostic accuracy and superior tissue characterization in several applications in the near future.

References

Alsop DC (1997) Phase insensitive preparation of single-shot RARE: application to diffusion imaging in humans. Magn Reson Med 38(4):527–533

Basser PJ, Pierpaoli C (1996) Microstructural and physiological features of tissues elucidated by quantitative-diffusion-tensor MRI. J Magn Reson B 111(3):209–219

Basser PJ, Pierpaoli C (1998) A simplified method to measure the diffusion tensor from seven MR images. Magn Reson Med 39(6):928–934

Basser PJ, Mattiello J et al (1994a) Estimation of the effective self-diffusion tensor from the NMR spin echo. J Magn Reson B 103(3):247–254

Basser PJ, Mattiello J et al (1994b) MR diffusion tensor spectroscopy and imaging. Biophys J 66(1):259–267

Baur A, Stabler A et al (1998) Diffusion-weighted MR imaging of bone marrow: differentiation of benign versus pathologic compression fractures. Radiology 207(2):349–356

Baur A, Huber A et al (2001) Diagnostic value of increased diffusion weighting of a steady-state free precession sequence for differentiating acute benign osteoporotic fractures from pathologic vertebral compression fractures. AJNR Am J Neuroradiol 22(2):366–372

Biffar A, Dietrich O et al (2010a) Diffusion and perfusion imaging of bone marrow. Eur J Radiol 76(3):323–328

Biffar A, Sourbron S et al (2010b) Combined diffusion-weighted and dynamic contrast-enhanced imaging of patients with acute osteoporotic vertebral fractures. Eur J Radiol 76(3):298–303

Biffar A, Sourbron S et al (2010c) Measurement of perfusion and permeability from dynamic contrast-enhanced MRI in normal and pathological vertebral bone marrow. Magn Reson Med 64(1):115–124

Biffar A, Baur-Melnyk A et al (2011a) Quantitative analysis of the diffusion-weighted steady-state free precession signal in vertebral bone marrow lesions. Invest Radiol 46(10):601–609

Biffar A, Schmidt GP et al (2011b) Quantitative analysis of vertebral bone marrow perfusion using dynamic contrast-enhanced MRI: initial results in osteoporotic patients with acute vertebral fracture. J Magn Reson Imaging 33(3):676–683

Brix G, Griebel J et al (2010) Tracer kinetic modelling of tumour angiogenesis based on dynamic contrast-enhanced CT and MRI measurements. Eur J Nucl Med Mol Imaging 37(Suppl 1):S30–S51

Brockstedt S, Moore JR et al (2000) High-resolution diffusion imaging using phase-corrected segmented echo-planar imaging. Magn Reson Imaging 18(6):649–657

Bruder H, Fischer H et al (1988) A new steady-state imaging sequence for simultaneous acquisition of two MR images with clearly different contrasts. Magn Reson Med 7(1):35–42

Buxton RB (1993) The diffusion sensitivity of fast steady-state free precession imaging. Magn Reson Med 29(2):235–243

Capuani S, Rossi C et al (2005) Diffusion tensor imaging to study anisotropy in a particular porous system: the trabecular bone network. Solid State Nucl Magn Reson 28(2–4):266–272

Chan WP, Liu YJ et al (2011) Relationship of idiopathic osteonecrosis of the femoral head to perfusion changes in

the proximal femur by dynamic contrast-enhanced MRI. Am J Roentgenol 196(3):637–643
Chen WT, Shih TT et al (2001) Vertebral bone marrow perfusion evaluated with dynamic contrast-enhanced MR imaging: significance of aging and sex. Radiology 220(1): 213–218
Chen WT, Shih TT et al (2002) Blood perfusion of vertebral lesions evaluated with gadolinium-enhanced dynamic MRI: in comparison with compression fracture and metastasis. J Magn Reson Imaging 15(3):308–314
Cohen Y, Assaf Y (2002) High *b*-value q-space analyzed diffusion-weighted MRS and MRI in neuronal tissues—a technical review. NMR Biomed 15(7–8):516–542
Courcoutsakis N, Spanoudaki A et al (2011) Perfusion parameters analysis of the vertebral bone marrow in patients with Ph(1-) chronic myeloproliferative neoplasms (Ph(neg) MPN): a dynamic contrast-enhanced MRI (DCE-MRI) study. J Magn Reson Imaging. doi:10.1002/jmri.22870 [Epub ahead of print]
D'Agostino F, Dell'Aia P et al (2010) Differentiation of normal and neoplastic bone tissue in dynamic gadolinium-enhanced magnetic resonance imaging: validation of a semiautomated technique. Radiol Med 115(5):804–814
Deoni SC, Peters TM et al (2004) Quantitative diffusion imaging with steady-state free precession. Magn Reson Med 51(2):428–433
Dietrich O (2008) Diffusion-weighted imaging and diffusion tensor imaging. In: Reiser MF, Semmler W, Hricak H (eds) Magnetic Resonance Tomography. Springer, Heidelberg, pp. 130−152
Dietrich O, Biffar A et al (2009) Diffusion-weighted imaging of bone marrow. Semin Musculoskelet Radiol 13(2):134–144
Dietrich O, Biffar A et al (2010) Technical aspects of MR diffusion imaging of the body. Eur J Radiol 76(3):314–322
Dietrich O, Baur-Melnyk A (2011) Diffusion-weighted MR imaging of the bone marrow and the spine. In: Taouli B (ed) Extra-cranial applications of diffusion-weighted MRI. Cambridge University Press, Cambridge, pp 144–161
Dyke JP, Aaron RK (2010) Noninvasive methods of measuring bone blood perfusion. Ann N Y Acad Sci 1192:95–102
Erlemann R, Reiser MF et al (1989) Musculoskeletal neoplasms: static and dynamic Gd-DTPA–enhanced MR imaging. Radiology 171(3):767–773
Gerdes CM, Kijowski R et al (2007) IDEAL imaging of the musculoskeletal system: robust water fat separation for uniform fat suppression, marrow evaluation, and cartilage imaging. AJR Am J Roentgenol 189(5):W284–W291
Glaser C, Weckbach S et al (2008) Musculoskeletal system. In: Reiser MF, Semmler W, Hricak H (eds) Magnetic resonance tomography. Springer, Heidelberg, pp 1079–1176
Griffith JF, Yeung DK et al (2005) Vertebral bone mineral density, marrow perfusion, and fat content in healthy men and men with osteoporosis: dynamic contrast-enhanced MR imaging and MR spectroscopy. Radiology 236(3):945–951
Griffith JF, Yeung DK et al (2009) Reproducibility of MR perfusion and (1)H spectroscopy of bone marrow. J Magn Reson Imaging 29(6):1438–1442
Griffith JF, Yeung DK et al (2011) Prediction of bone loss in elderly female subjects by MR perfusion imaging and spectroscopy. Eur Radiol 21(6):1160–1169
Gudbjartsson H, Maier SE et al (1996) Line scan diffusion imaging. Magn Reson Med 36(4):509–519
Gyngell ML (1988) The application of steady-state free precession in rapid 2DFT NMR imaging: FAST and CE-FAST sequences. Magn Reson Imaging 6(4):415–419
Hahn EL (1950) Spin echoes. Phys Rev 80(4):580–594
Jackson A, Buckley DL et al (eds) (2005) Dynamic contrast-enhanced magnetic resonance imaging in oncology. Medical radiology—diagnostic imaging. Springer, Heidelberg
Jensen JH, Helpern JA (2010) MRI quantification of non-Gaussian water diffusion by kurtosis analysis. NMR Biomed 23(7):698–710
Kind T, Houtzager I et al (2010) Evaluation of model-independent deconvolution techniques to estimate blood perfusion. Conf Proc IEEE Eng Med Biol Soc 2602–2607
Koh DM, Collins DJ et al (2011) Intravoxel incoherent motion in body diffusion-weighted MRI: reality and challenges. AJR Am J Roentgenol 196(6):1351–1361
Korosec FR, Frayne R et al (1996) Time-resolved contrast-enhanced 3D MR angiography. Magn Reson Med 36(3): 345–351
Lambregts DM, Maas M et al (2011) Whole-body diffusion-weighted magnetic resonance imaging: current evidence in oncology and potential role in colorectal cancer staging. Eur J Cancer 47(14):2107–2116
Le Bihan D (1988) Intravoxel incoherent motion imaging using steady-state free precession. Magn Reson Med 7(3): 346–351
Le Bihan D, Breton E et al (1986) MR imaging of intravoxel incoherent motions: application to diffusion and perfusion in neurologic disorders. Radiology 161(2):401–407
Le Bihan D, Breton E et al (1988) Separation of diffusion and perfusion in intravoxel incoherent motion MR imaging. Radiology 168(2):497–505
Le Roux P (2002) Non-CPMG Fast Spin Echo with full signal. J Magn Reson 155(2):278–292
Lee H, Price RR (1994) Diffusion imaging with the MP-RAGE sequence. J Magn Reson Imaging 4(6):837–842
Lee JH, Dyke JP et al (2009) Assessment of bone perfusion with contrast-enhanced magnetic resonance imaging. Orthop Clin North Am 40(2):249–257
Li X, Yu A et al (2012) Quantitative characterization of bone marrow edema pattern in rheumatoid arthritis using 3 Tesla MRI. J Magn Reson Imaging 35(1):211–217
Lim RP, Shapiro M et al (2008) 3D time-resolved MR angiography (MRA) of the carotid arteries with time-resolved imaging with stochastic trajectories: comparison with 3D contrast-enhanced Bolus-Chase MRA and 3D time-of-flight MRA. AJNR Am J Neuroradiol 29(10):1847–1854
Luypaert R, Boujraf S et al (2001) Diffusion and perfusion MRI: basic physics. Eur J Radiol 38(1):19–27
Ma HT, Griffith JF et al (2010) Modified brix model analysis of bone perfusion in subjects of varying bone mineral density. J Magn Reson Imaging 31(5):1169–1175
Meier P, Zierler KL (1954) On the theory of the indicator-dilution method for measurement of blood flow and volume. J Appl Physiol 6(12):731–744
Merboldt KD, Hanicke W et al (1985) Self-Diffusion NMR Imaging Using Stimulated Echoes. J Magn Reson 64(3): 479–486
Merboldt KD, Bruhn H et al (1989) MRI of "diffusion" in the human brain: new results using a modified CE-FAST sequence. Magn Reson Med 9(3):423–429

Moehler TM, Hawighorst H et al (2001) Bone marrow microcirculation analysis in multiple myeloma by contrast-enhanced dynamic magnetic resonance imaging. Int J Cancer 93(6):862–868

Montazel JL, Divine M et al (2003) Normal spinal bone marrow in adults: dynamic gadolinium-enhanced MR imaging. Radiology 229(3):703–709

Norris DG (2007) Selective parity RARE imaging. Magn Reson Med 58(4):643–649

Norris DG, Bornert P et al (1992) On the application of ultra-fast RARE experiments. Magn Reson Med 27(1): 142–164

Nosas-Garcia S, Moehler T et al (2005) Dynamic contrast-enhanced MRI for assessing the disease activity of multiple myeloma: a comparative study with histology and clinical markers. J Magn Reson Imaging 22(1):154–162

Oppelt A, Graumann R et al (1986) FISP—a new fast MRI sequence. Electromedica 54:15–18

Ostergaard L (2004) Cerebral perfusion imaging by bolus tracking. Top Magn Reson Imaging 15(1):3–9

Petersen ET, Zimine I et al (2006) Non-invasive measurement of perfusion: a critical review of arterial spin labelling techniques. Br J Radiol 79(944):688–701

Pipe JG, Farthing VG et al (2002) Multishot diffusion-weighted FSE using PROPELLER MRI. Magn Reson Med 47(1): 42–52

Rahmouni A, Montazel JL et al (2003) Bone marrow with diffuse tumor infiltration in patients with lymphoproliferative diseases: dynamic gadolinium-enhanced MR imaging. Radiology 229(3):710–717

Robson MD, Anderson AW et al (1997) Diffusion-weighted multiple shot echo planar imaging of humans without navigation. Magn Reson Med 38(1):82–88

Rossi C, Capuani S et al (2005) DTI of trabecular bone marrow. Magn Reson Imaging 23(2):245–248

Savvopoulou V, Maris TG et al (2011) Degenerative endplate changes of the lumbosacral spine: dynamic contrast-enhanced MRI profiles related to age, sex, and spinal level. J Magn Reson Imaging 33(2):382–389

Shih TT, Liu HC et al (2004) Correlation of MR lumbar spine bone marrow perfusion with bone mineral density in female subjects. Radiology 233(1):121–128

Silbernagl S, Despopoulos A (2008) Color atlas of physiology. Thieme, Stuttgart

Sourbron S (2010) Technical aspects of MR perfusion. Eur J Radiol 76(3):304–313

Sourbron SP, Buckley DL (2012) Tracer kinetic modelling in MRI: estimating perfusion and capillary permeability. Phys Med Biol 57(2):R1–R33

Stejskal EO, Tanner JE (1965) Spin diffusion measurements: spin echoes in the presence of a time-dependent field gradient. J Chem Phy 42(1):288–292

Takahara T, Imai Y et al (2004) Diffusion weighted whole body imaging with background body signal suppression (DWIBS): technical improvement using free breathing, STIR and high resolution 3D display. Radiat Med 22(4):275–282

Taylor DG, Bushell MC (1985) The spatial-mapping of translational diffusion-coefficients by the NMR imaging technique. Phys Med Biol 30(4):345–349

Tokuda O, Hayashi N et al (2005) Dynamic contrast-enhanced perfusion MR imaging of diseased vertebrae: analysis of three parameters and the distribution of the time-intensity curve patterns. Skeletal Radiol 34(10):632–638

Turner R, Le Bihan D et al (1990) Echo-planar imaging of intravoxel incoherent motion. Radiology 177(2):407–414

Vanel D (2004) MRI of bone metastases: the choice of the sequence. Cancer Imaging 4(1):30–35

Wu EX, Buxton RB (1990) Effect of diffusion on the steady-state magnetization with pulsed field gradients. J Magn Reson 90(2):243–253

Wu LM, Gu HY et al (2011) Diagnostic value of whole-body magnetic resonance imaging for bone metastases: a systematic review and meta-analysis. J Magn Reson Imaging 34(1):128–135

Zierler KL (1962) Theoretical basis of indicator-dilution methods for measuring flow and volume. Circ Res 10(3):393–407

Zierler KL (1965) Equations for measuring blood flow by external monitoring of radioisotopes. Circ Res 16:309–321